ARTICLE

doi:10.1038/nature09504

Selective inhibition of BET bromodomains

Panagis Filippakopoulos[1]*, Jun Qi[2]*, Sarah Picaud[1]*, Yao Shen[3], William B. Smith[2], Oleg Fedorov[1], Elizabeth M. Morse[2], Tracey Keates[1], Tyler T. Hickman[4], Ildiko Felletar[1], Martin Philpott[1], Shonagh Munro[5], Michael R. McKeown[2,6], Yuchuan Wang[7], Amanda L. Christie[8], Nathan West[2], Michael J. Cameron[4], Brian Schwartz[4], Tom D. Heightman[1], Nicholas La Thangue[5], Christopher A. French[4], Olaf Wiest[3], Andrew L. Kung[8,9], Stefan Knapp[1,5] & James E. Bradner[2,6]

Epigenetic proteins are intently pursued targets in ligand discovery. So far, successful efforts have been limited to chromatin modifying enzymes, or so-called epigenetic 'writers' and 'erasers'. Potent inhibitors of histone binding modules have not yet been described. Here we report a cell-permeable small molecule (JQ1) that binds competitively to acetyl-lysine recognition motifs, or bromodomains. High potency and specificity towards a subset of human bromodomains is explained by co-crystal structures with bromodomain and extra-terminal (BET) family member BRD4, revealing excellent shape complementarity with the acetyl-lysine binding cavity. Recurrent translocation of BRD4 is observed in a genetically-defined, incurable subtype of human squamous carcinoma. Competitive binding by JQ1 displaces the BRD4 fusion oncoprotein from chromatin, prompting squamous differentiation and specific antiproliferative effects in BRD4-dependent cell lines and patient-derived xenograft models. These data establish proof-of-concept for targeting protein–protein interactions of epigenetic 'readers', and provide a versatile chemical scaffold for the development of chemical probes more broadly throughout the bromodomain family.

Gene regulation is fundamentally governed by reversible, non-covalent assembly of macromolecules[1]. Signal transduction to RNA polymerase requires higher-ordered protein complexes, spatially regulated by assembly factors capable of interpreting the post-translational modification states of chromatin[2]. Readers of epigenetic marks are structurally diverse proteins each possessing one or more evolutionarily conserved effector modules, which recognize covalent modifications of histone proteins or DNA. The ε-N-acetylation of lysine residues (Kac) on histone tails is associated with an open chromatin architecture and transcriptional activation[3]. Context-specific molecular recognition of acetyl-lysine is principally mediated by bromodomains.

Bromodomain-containing proteins are of substantial biological interest, as components of transcription factor complexes and determinants of epigenetic memory[4]. There are 41 diverse human proteins containing a total of 57 bromodomains. Despite large sequence variations, all bromodomain modules share a conserved fold comprising a left-handed bundle of four α helices (α_Z, α_A, α_B, α_C), linked by diverse loop regions (ZA and BC loops) that contribute to substrate specificity. Co-crystal structures with peptidic substrates showed that the acetyl-lysine is recognized by a central hydrophobic cavity and is anchored by a hydrogen bond with an asparagine residue present in most bromodomains[5]. The BET family (BRD2, BRD3, BRD4 and BRDT) shares a common domain architecture featuring two amino-terminal bromodomains that exhibit high levels of sequence conservation, and a more divergent carboxy-terminal recruitment domain (Supplementary Fig. 1)[6].

Recent research has established a compelling rationale for targeting BRD4 in cancer. BRD4 remains bound to transcriptional start sites of genes expressed during the M/G1 transition, influencing mitotic progression[4]. BRD4 is also a critical mediator of transcriptional elongation, functioning to recruit the positive transcription elongation factor complex (P-TEFb)[7,8]. Cyclin-dependent kinase-9, a core component of P-TEFb[9–11], is a validated target in chronic lymphocytic leukaemia[12], and has recently been linked to c-Myc-dependent transcription[13]. Thus, BRD4 recruits P-TEFb to mitotic chromosomes resulting in increased expression of growth-promoting genes[14].

Importantly, BRD4 has recently been identified as a component of a recurrent t(15;19) chromosomal translocation in an aggressive form of human squamous carcinoma[15,16]. Such translocations express the tandem N-terminal bromodomains of BRD4 as an in-frame chimaera with the NUT (nuclear protein in testis) protein, genetically defining the so-called NUT midline carcinoma (NMC). Functional studies in patient-derived NMC cell lines have validated the essential role of the BRD4–NUT oncoprotein in maintaining the characteristic proliferation advantage and differentiation block of this uniformly fatal malignancy[17]. Notably, RNA silencing of BRD4–NUT arrests proliferation and prompts terminal squamous differentiation. These observations underscore the broad utility and immediate therapeutic potential of a direct-acting inhibitor of human bromodomain proteins.

A selective and potent inhibitor of BET family bromodomains

A major collaborative focus of our research groups concerns the development of chemical probes[18,19] and the optimization of therapeutic leads for the translation of small-molecule modulators of epigenetic targets as cancer therapeutics. Motivated by the above rationale, we have developed biochemical platforms for the identification of new inhibitors of bromodomain isoforms using high-throughput screening, as well as the annotation of putative ligands emerging from collaborative and published research. In the course of these studies, we learned of an

[1]Department of Clinical Medicine, Structural Genomics Consortium, University of Oxford, Old Road Campus, Roosevelt Drive, Oxford OX3 7DQ, UK. [2]Department of Medical Oncology, Dana-Farber Cancer Institute, Harvard Medical School, 44 Binney Street, Boston, Massachusetts 02115, USA. [3]Walther Cancer Research Center and Department of Chemistry and Biochemistry, University of Notre Dame, Notre Dame, Indiana 46556, USA. [4]Department of Pathology, Brigham & Women's Hospital, Harvard Medical School, 75 Francis Street, Boston, Massachusetts 02115, USA. [5]Department of Clinical Pharmacology, University of Oxford, Old Road Campus, Roosevelt Drive, Oxford OX3 7DQ, UK. [6]Department of Medicine, Harvard Medical School, 25 Shattuck Street, Boston, Massachusetts 02115, USA. [7]Department of Imaging, Dana-Farber Cancer Institute, Harvard Medical School, 44 Binney Street, Boston, Massachusetts 02115, USA. [8]Lurie Family Imaging Center, Dana-Farber Cancer Institute, Harvard Medical School, 44 Binney Street, Boston, Massachusetts 02115, USA. [9]Department of Pediatric Oncology, Dana-Farber Cancer Institute and Children's Hospital, Boston, Harvard Medical School, 44 Binney Street, Boston, Massachusetts 02115, USA.
*These authors contributed equally to this work.

observation by Mitsubishi Pharmaceuticals that simple thienodiazepines possessed binding activity for BRD4 (ref. 20). Previous research from this group indicates that these compounds emerged from anti-inflammatory phenotypic studies, such as inhibition of CD28 co-stimulation as a means of treating autoimmune diseases[21,22]. A rich literature has established the synthetic accessibility and favourable pharmacological properties of this privileged class of drug-like small molecules[23]. Indeed, the core scaffold described appears in FDA-approved substances such as alprazolam and triazolam.

Inferring structure–activity relationships also derived from molecular modelling of candidate ligands within the binding pocket of the apo crystal structure of the first bromodomain of BRD4 (hereafter referred to as BRD4(1); Protein Data Bank code 2OSS), we designed a prototype ligand, JQ1 (Fig. 1a). JQ1 is a novel thieno-triazolo-1,4-diazepine, possessing an appended, bulky *t*-butyl ester functional group at C6 in order to (1) allow for additional pendant group diversity, as needed, and (2) to mitigate binding to the central benzodiazepine receptor as predicted by published structure–activity relationships[23]. We first established a high-yielding, seven-step synthetic route to access racemic JQ1 (hereafter referred to as JQ1) and derivatives (scheme 1 in Supplementary Methods). We have also identified a route to synthesize each enantiomer, (+)-JQ1 and (−)-JQ1 (scheme 2 in Supplementary Methods).

To establish a biochemical platform for comprehensive selectivity screening, all human bromodomains were subcloned into bacterial expression vectors. Testing of an average of 15 expression constructs per bromodomain resulted in the identification of 37 expression systems that yielded soluble protein suitable for specificity screening and covered all bromodomain subfamilies (Supplementary Table 1). Because the specific substrates of most bromodomains are unknown, a general binding assay based on differential scanning fluorimetry (DSF) was implemented[24]. Binding of (+)-JQ1 significantly increased the thermal stability of all bromodomains of the BET family (Fig. 1b and Supplementary Table 2) with ΔT_m^{obs} values between 4.2 °C (BRDT(1)) and 10.1 °C (BRD4(1)). No significant stability shifts were detected for bromodomains outside the BET family, indicating that this ligand is highly selective. In contrast, the stereoisomer (−)-JQ1 showed no significant interaction with any bromodomain present in our panel.

Within a family of proteins a linear correlation between DSF ΔT_m^{obs} values and binding constants has been observed, with temperature shifts larger than 6 °C corresponding to compounds with nanomolar

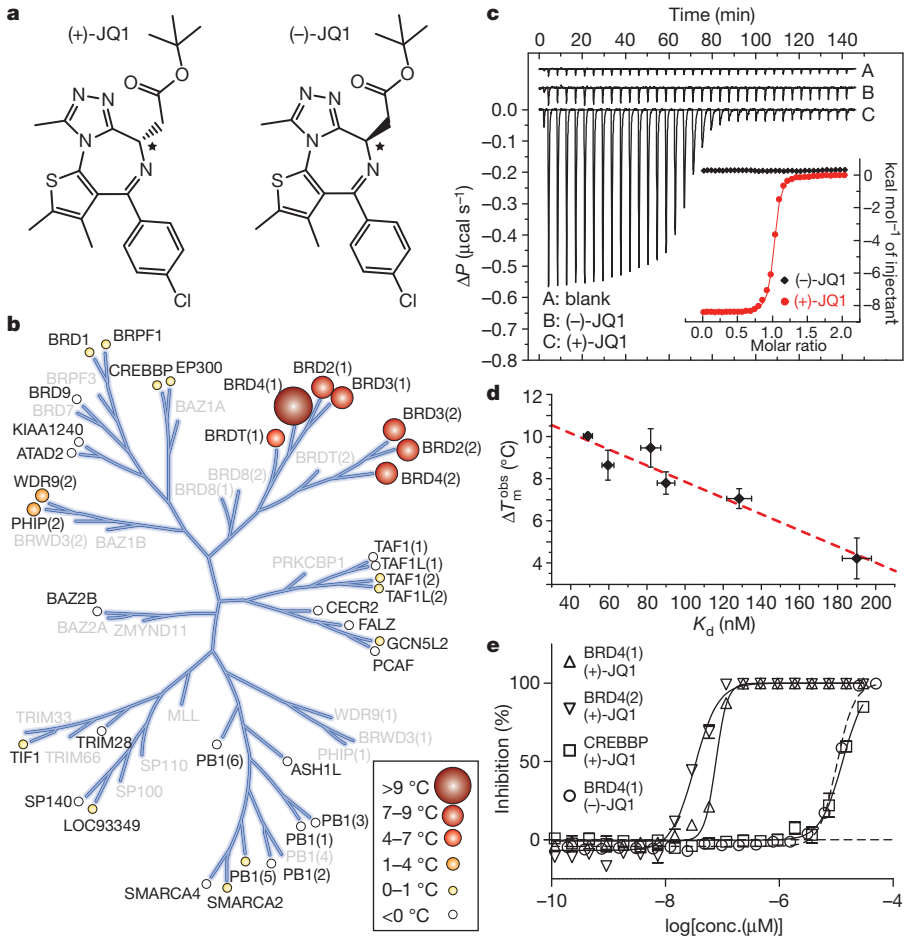

Figure 1 | Structure and selectivity of JQ1. **a**, Structure of the two JQ1 stereoisomers. The stereocentre at C6 is indicated by an asterisk. **b**, Assessment of inhibitor selectivity using differential scanning fluorimetry (DSF). Shown are averaged temperature shifts (ΔT_m^{obs}) in degrees Celsius upon binding of 10 μM (+)-JQ1. The temperature shifts are represented by spheres as indicated in the inset. Screened bromodomains are labelled and proteins not included in the selectivity panel are shown in grey. (−)-JQ1 did not reveal any significant temperature shifts to any of the screened bromodomains. **c**, Isothermal titration calorimetry (ITC). Differential power (ΔP) data time course of raw injection heats are shown for a blank titration of BRD4(1) into buffer (A), and reverse titrations using the inactive isomer (−)-JQ1 (B) and the active isomer (+)-JQ1 (C). The inset shows normalized binding enthalpies corrected for the heat of dilution as a function of binding site saturation (symbols as indicated in the inset). Solid lines represent a nonlinear least squares fit using a single-site binding model. **d**, Thermal shifts (ΔT_m^{obs}) show good correlation to dissociation constants (K_d) determined by ITC for the BET bromodomains. The dotted red line represents a least squares fit with an R of 96%. The ΔT_m^{obs} data represent the mean ± s.d. ($n = 3$). Error for ITC data was based on deviations to least squares fit described in **c**. **e**, Competitive displacement of a histone peptide from human bromodomains is exhibited by JQ1 using a bead-based proximity assay. Alpha-screen titrations monitoring the displacement of a tetra-acetylated histone H4 peptide by JQ1 isomers using the bromodomains BRD4(1), BRD4(2) or of an acetylated H3 peptide using CREBBP are shown.

dissociation constants (K_d)[25,26]. Because the sensitivity of this assay may vary between different protein families, isothermal titration calorimetry (ITC) was used to determine binding constants precisely. Enantiomerically pure (+)-JQ1 bound with a K_d of about 50 nM and 90 nM to the first and second bromodomains of BRD4, respectively (Fig. 1c and Supplementary Table 3). Comparable binding to both domains of BRD3 was observed, whereas the first bromodomains of BRDT and BRD2 revealed about threefold weaker binding. Affinities determined by ITC and ΔT_m^{obs} values showed very good correlation (Fig. 1d). Importantly, (+)-JQ1 showed no detectable binding to bromodomains that exhibited minimal temperature shifts, such as WDR9(2) and CREBBP.

To assess whether (+)-JQ1 binding was competitive with acetyl-lysine, we adapted a luminescence proximity homogeneous assay (alpha-screen)[27] to the BET bromodomains. Binding of a tetra-acetylated histone H4 peptide to BRD4 was strongly inhibited by (+)-JQ1, with half-maximum inhibitory concentration (IC_{50}) values of 77 nM and 33 nM for the first and second bromodomain, respectively (Fig. 1e). The IC_{50} for the (−)-JQ1 stereoisomer against BRD4(1) and for (+)-JQ1 against CREBBP were both estimated to be above 10,000 nM (Fig. 1e). Thus, (+)-JQ1 represents a potent, highly specific and Kac-competitive inhibitor for the BET family of bromodomains.

(+)-JQ1 binds to the Kac binding site of BET bromodomains

To establish the binding mode of JQ1 we determined co-crystal structures using racemic material and purified, recombinant BRD4(1) and BRD2(2) (for data collection and refinement statistics see Supplementary Table 4). The determined high-resolution structures revealed that only the (+)-JQ1 enantiomer bound directly into the Kac binding site (Figs 2 and 3a, b). Similar to interactions observed in acetyl-lysine complexes[28], the triazole ring formed a hydrogen bond with the evolutionarily conserved asparagine (Asn 140 in BRD4(1) and Asn 429 in BRD2(2); Fig. 2a). The inhibitor showed an extraordinary shape complementarity with the Kac binding site, occupying the entire binding pocket (Fig. 2c, d). In both complexes, ligand binding was stabilized by hydrophobic interactions with conserved BET residues in the ZA- and BC-loop regions (Fig. 3a, b). Structural and sequence comparison showed high conservation of the BET Kac binding pocket, but revealed a number of differences in loop regions lining the binding cavity that could be explored for future development of isoform-specific inhibitors (Fig. 3a–c).

Docking of either isomer of JQ1 to BRD4(1) resulted in excellent fit of (+)-JQ1 in a position of perfect overlap to the crystallographically determined binding mode, whereas (−)-JQ1 resulted in an energetically unfavourable conformation with significant distortion of the diazepine ring system due to steric clashes with residues of the ZA-loop region (Fig. 3d). To explore the dynamic features of BET bromodomains, we carried out 20-ns molecular dynamics simulations of BRD4(1) in the absence and presence of (+)-JQ1. The simulations revealed little displacement of the protein helices, but the loop regions surrounding the acetyl-lysine binding site showed significant conformational

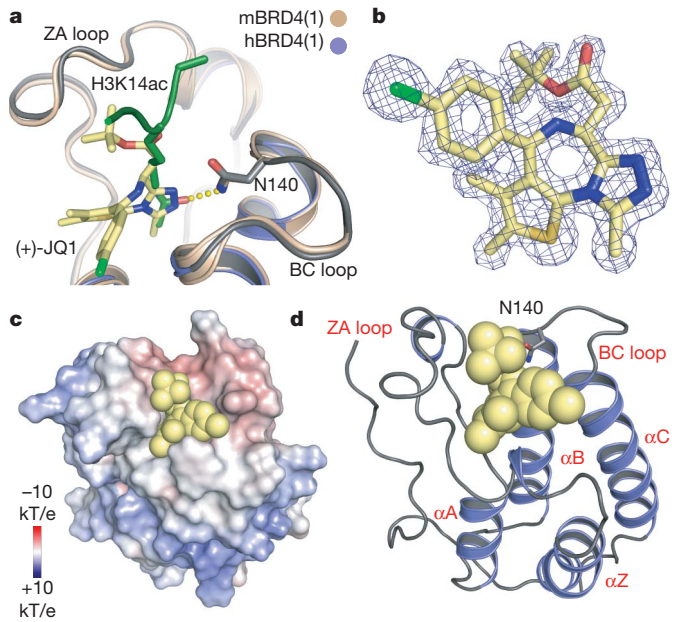

Figure 2 | Characterization of BET complexes with (+)-JQ1. **a**, Superimposition of the mouse BRD4(1)–H3K14ac peptide complex[28] with the human BRD4(1)–(+)-JQ1 complex structure. The hydrogen bond formed to the conserved asparagine (N140) in the peptide complex is shown as yellow dots. **b**, $2F_o - F_c$ map of (+)-JQ1 in complex with BRD4(1) contoured at 2σ. **c**, Electrostatic surface of BRD4(1) in complex with (+)-JQ1. The ligand is shown as a Corey–Pauling–Koltun (CPK) model demonstrating the excellent shape complementarity with the protein acetylated lysine receptor site. **d**, Ribbon diagram of the complex of human BRD4(1) with (+)-JQ1 in CPK representation. The main secondary structural elements and the conserved active site asparagine side chain (N140) are labelled.

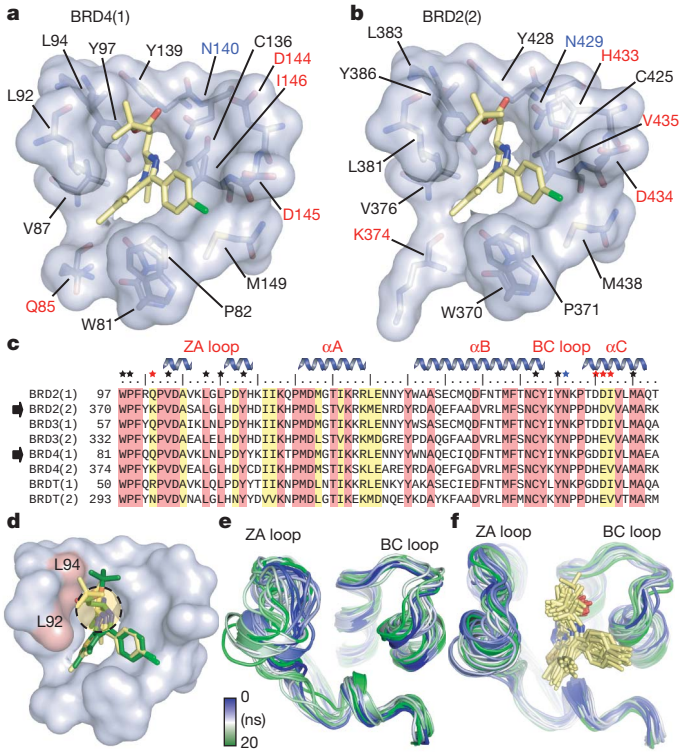

Figure 3 | Binding site comparison between N- and C-terminal bromodomains in complex with (+)-JQ1. **a**, The acetyl-lysine binding pocket of BRD4(1) is shown as a semi-transparent surface with contact residues labelled and depicted in stick representation. Carbon atoms in (+)-JQ1 are coloured yellow to distinguish them from protein residues. Distinguishing surface residues are shown in red; the family conserved asparagine is shown in blue. **b**, The acetyl-lysine binding pocket of BRD2(2) is shown in identical representation and orientation as described in **a**. **c**, Protein sequence alignment of the human BET sub-family highlighting conserved (red) and similar (yellow) residues. Major bromodomain structural elements are shown. The side-chain contacts with (+)-JQ1 are annotated with a black star. Contacts which differ between the N- and C-terminal BET bromodomains (red star) are highlighted. The conserved asparagine is indicated by a blue star. **d**, Models of (+)-JQ1 (in yellow) and (−)-JQ1 (in green) docked into the BRD4(1) binding site. The steric clashes of the (−)-JQ1 stereoisomer with Leu 92 and Leu 94 are highlighted in red. **e**, Molecular dynamics simulation demonstrating the flexibility of the ZA and BC loops of the BRD4(1) apo-structure. Shown is the backbone of BRD4(1) during a 20-ns simulation as snapshots separated by 1-ns intervals. The different structures are distinguished by colours changing from blue to green as indicated in the inset. **f**, Molecular dynamics simulation of the BRD4(1)–(+)-JQ1 complex depicted in 1-ns snapshots as described in **e**.

flexibility. Furthermore, these loops were much more flexible in the absence (Fig. 3e) than in the presence (Fig. 3f) of the inhibitor, indicating that (+)-JQ1 stabilized the Kac binding cavity. In all cases, molecular dynamics simulation energies converged (Supplementary Fig. 2).

JQ1 displaces BRD4 from nuclear chromatin in cells

To establish whether JQ1 binds bromodomains competitively with chromatin in a cellular environment, we performed fluorescence recovery after photobleaching (FRAP) experiments. Previous research has demonstrated the utility of FRAP in assessing the pace of lateral redistribution of human bromodomains[17,29]. Human osteosarcoma cells (U2OS) transfected with GFP–BRD4 show a time-dependent recovery of fluorescence intensity (Fig. 4a, b). In the presence of JQ1 (500 nM), the observed recovery is immediate, indicating displaced and freely diffusing nuclear BRD4 (Fig. 4a, b). Cellular FRAP studies confirmed that the effects on the mobile fraction of BRD4 are limited to the biochemically active (+)-JQ1 stereoisomer (Supplementary Fig. 3).

Having demonstrated potent, selective binding to BRD4 in homogeneous and cell-based assays, we became interested to explore the effects of JQ1 on disease-relevant phenotypes. Previous studies have established that the pathogenic BRD4–NUT fusion protein arising from the t(15;19) translocation in NMC binds avidly to discrete foci of acetylated chromatin, conferring a proliferative advantage and differentiation block[17]. Using FRAP, we assessed the ability of JQ1 to target directly the BRD4–NUT oncoprotein. Compared to a vehicle control, JQ1 (500 nM) markedly accelerated time to half fluorescence recovery in photobleached regions of cells transfected with GFP–BRD4–NUT (Fig. 4c, d). Notably, no effect was observed on redistribution of GFP–NUT (Supplementary Fig. 3). These data are consistent with competitive binding of JQ1 to BRD4 in cultured cells.

JQ1 induces differentiation and growth arrest in NMC

Direct inhibition of gene products expressed from recurrent, oncogenic translocations is a validated therapeutic approach in cancer[30,31]. We thus endeavoured to establish the consequences of competitive inhibition of BRD4–NUT in NMC. A characteristic feature of NMC is the appearance of discrete nuclear speckles of the BRD4–NUT oncoprotein by NUT-directed immunohistochemistry[32]. Treatment of the patient-derived 797 NMC cell line for 48 h with JQ1 (500 nM) effaces nuclear foci, producing diffuse nuclear NUT staining by immunohistochemistry (Supplementary Fig. 3e). In a dose- and time-dependent manner, JQ1 provokes a differentiation phenotype in NMC cell lines,

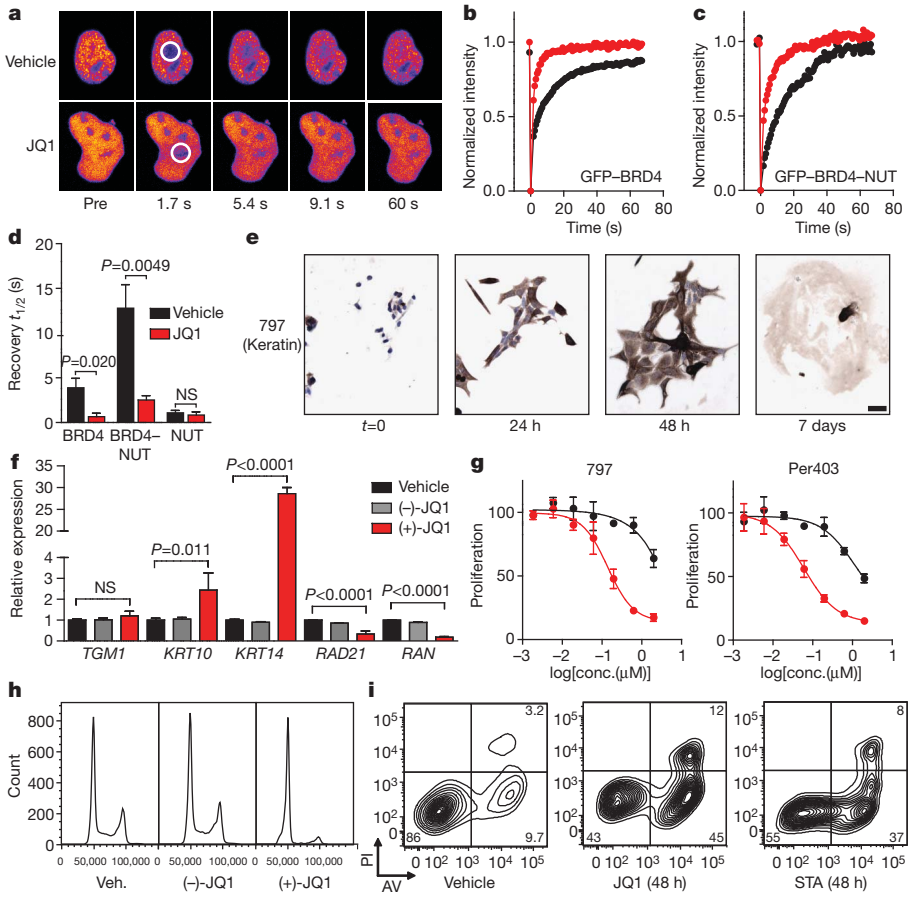

Figure 4 | JQ1 binds BRD4 competitively with chromatin resulting in differentiation and growth arrest of NMC cells. **a**, Fluorescence recovery after photobleaching (FRAP) of GFP–BRD4 demonstrates enhanced recovery in the presence of JQ1. Nuclei are false-coloured in proportion to fluorescence intensity. White circles indicate target regions of photobleaching. **b**, **c**, JQ1 accelerates fluorescence recovery in FRAP experiments performed with transfected GFP–BRD4 (**b**) and GFP–BRD4–NUT (**c**). **d**, Quantitative comparison of time to half-maximal fluorescence recovery for FRAP studies (**b**, **c**, Supplementary Fig. 3a). Data represent the mean ± s.d. ($n = 5$), and are annotated with *P*-values as obtained from a two-tailed *t*-test. NS, not significant. **e**, Differentiation of NMC cells by JQ1 (500 nM) is prompt and characterized by a marked increase in cytokeratin expression (mouse anti-cytokeratin clone AE1/AE3; ×10, scale bar is 50 μm). **f**, Comparative gene expression studies of (+)-JQ1 (red; 250 nM, 48 h) versus (−)-JQ1 (grey; 250 nM, 48 h) and vehicle (black) confirm squamous differentiation. Data represent the mean ± s.d. ($n = 3$), and are annotated with *P*-values as obtained from a two-tailed *t*-test. **g**, Growth effects of BRD4 inhibition on BRD4–NUT-dependent cell lines. Cells were incubated with (+)-JQ1 (red circles) or (−)-JQ1 (black circles) and monitored for proliferation after 72 h. (+)-JQ1 uniquely attenuates proliferation by NMC cell lines. Data are presented as mean ± s.d. ($n = 3$). Curve fit was calculated by logistical regression. **h**, Flow cytometry for DNA content in NMC 797 cells. (+)-JQ1 (250 nM, 48 h) induces a G1 arrest compared to (−)-JQ1 (250 nM) and vehicle control. Data are presented as a histogram of nuclear fluorescence intensity. **i**, Flow cytometric analysis of NMC 797 squamous carcinoma cells treated with vehicle, JQ1 or staurosporine (STA), as indicated. AV, annexin-V; PI, propidium iodide.

featuring cell spreading and flattening, open chromatin and striking spindle morphology (Fig. 4e and Supplementary Fig. 4). Differentiation is prompt (<24 h) and characterized by marked changes in cell shape accompanied by markedly augmented expression of cytokeratin, a hallmark of squamous differentiation (Fig. 4e). After 7 days in culture with submicromolar exposures to JQ1, terminal differentiation is observed. In this manner, JQ1 phenocopies the morphological changes and increased keratin expression observed with BRD4–NUT silencing by RNA interference (Supplementary Fig. 5)[17]. Corroborating these studies, expression analysis of three canonical squamous tissue genes by RT–PCR identified marked (30-fold) induction of keratin-14 by (+)-JQ1 in NMC 797 cells (Fig. 4f). The modest induction of keratin-10 without affecting epidermal transglutaminase (TGM1) may indicate differentiation towards thoracic squamous epithelium, consistent with the mediastinal primary tumour from which NMC 797 cells derive[33]. Induction of differentiation with intense keratin staining is progressive over 72 h, as determined by quantitative immunohistochemistry analysis (Supplementary Fig. 6). Supporting an on-target mechanism-of-action, the (−)-JQ1 enantiomer is comparatively inactive in NMC, and a non-BRD4-dependent squamous carcinoma cell line (TE10) fails to exhibit differentiation effects of active JQ1 (Supplementary Fig. 4c).

In BRD4-dependent NMC cells, differentiation is expectedly accompanied by growth arrest, as demonstrated by reduced Ki67 staining (Supplementary Fig. 7), sustained inhibition of proliferation (Fig. 4g; Supplementary Fig. 8) and G1 cell-cycle arrest (Fig. 4h). To understand further the observed G1 arrest and to confirm an effect of JQ1 on known BRD4-dependent genes, we performed quantitative RT–PCR for *RAD21* and *RAN* (ref. 4). (+)-JQ1 potently decreased expression of both BRD4 target genes, whereas (−)-JQ1 had no effect (Fig. 4f). Early and late apoptosis were assessed with annexin-V and propidium iodide staining to ascertain whether the antiproliferative effect and irreversible differentiation was accompanied by cell death. Indeed, JQ1 induces immediate and progressive apoptosis in BRD4-dependent human carcinoma cells, without triggering significant growth arrest or cell death in cell lines lacking the BRD–NUT fusion (Supplementary Figs 8 and 9).

Antitumour efficacy of JQ1 in xenograft models of NMC

To determine whether JQ1 could attenuate the growth of BRD4-dependent carcinoma as a single agent *in vivo*, we developed three xenograft models of NMC in mice. First, short-term treatment studies were performed in NMC 797 xenografts with positron-emission tomography (PET) imaging of ^{18}F-fluorodeoxyglucose (FDG) uptake as a primary endpoint to explore whether activity of JQ1 could be demonstrated by non-invasive imaging. Matched cohorts of mice with established tumours were randomized to treatment with JQ1 (50 mg kg^{-1}) or vehicle, administered by daily intraperitoneal injection. Before randomization, and after 4 days of therapy, mice were evaluated by FDG-PET imaging. A marked reduction in FDG uptake was observed with JQ1 treatment, whereas vehicle-treated mice demonstrated progressive disease (Fig. 5a). Tumour-volume measurements confirmed a reduction in tumour growth with JQ1 treatment (Fig. 5b and Supplementary Fig. 10). JQ1 was well tolerated at this dose and schedule without overt signs of toxicity or weight loss (Supplementary Fig. 10b).

To confirm that the antineoplastic effect observed with JQ1 treatment was associated with target engagement, sectioned tumour tissue was examined for the BRD4–NUT oncoprotein. As presented in Supplementary Fig. 11, JQ1 treatment resulted in effacement of NUT nuclear speckles, consistent with competitive binding to nuclear chromatin. Cell spreading and increased keratin expression confirmed induction of squamous differentiation (Fig. 5c). Decreased nuclear Ki67 and increased TUNEL staining in treated animals confirmed an ongoing antiproliferative, pro-apoptotic effect (Supplementary Fig. 11). To quantify the pharmacodynamic biomarker of tumour keratin expression, we established protocols for automated immunohistochemistry image acquisition and analysis. Paired samples from treated and untreated animals were prepared and analysed using standardized protocols and commercially available software (ImageScope; Aperio Technologies), demonstrating that JQ1 induced strong (grade 3+) keratin expression in NMC 797 xenografts (Supplementary Fig. 12).

In parallel with these studies, we had occasion to care for a 29-year-old patient with widely metastatic BRD4–NUT-positive NMC arising from the mediastinum. With the goal of developing a more clinically relevant disease model, we established short-term cultures (11060 cells) using discarded clinical material obtained from pleural fluid draining from a palliative chest tube. As presented in Supplementary Fig. 13, *in vitro* studies confirmed the stereospecific, potent effect of (+)-JQ1 on cellular viability (IC_{50} = 4 nM), growth and cell cycle progression. Four animals engrafted with patient-derived tumour material developed measurable disease, which was strongly FDG-avid by PET imaging (Fig. 5d). Animals were randomly assigned to vehicle or (+)-JQ1 treatment. Before treatment and after 4 days of therapy, mice were evaluated by PET imaging. A marked response in FDG uptake was observed with (+)-JQ1 treatment, whereas vehicle-treated animals demonstrated progressive disease (Fig. 5e). Tumour material prepared for quantitative immunohistochemistry analysis demonstrated induction of keratin expression after (+)-JQ1 treatment (Fig. 5f, g and Supplementary Fig. 14) in this minimally passaged NMC xenograft model.

To confirm the translational potential of direct-acting BRD4 inhibition in NMC, we further adapted the patient-derived 11060 cells to expansion *in vivo*, and performed definitive efficacy studies. Marked tumour regression and prolonged overall survival were observed, after only 18 days of well-tolerated therapy with (+)-JQ1 (Fig. 5h, i). These results were recapitulated in a third NMC xenograft model, using Per403 cells (Fig. 5j, k and Supplementary Fig. 15). Together, these data establish *in vivo* proof-of-concept for targeting BRD4 with JQ1 in NMC.

Discussion

Across the complex landscape of the cancer genome, recurrent chromosomal rearrangements comprise a compelling subset of clear, genetic targets in cancer. As evidenced by the successful development of first- and second-generation kinase inhibitors targeting BCR–ABL in chronic myelogenous leukaemia, well-characterized probe compounds[34,35], high-resolution crystallographic data[36], translational research studies[37], and informative murine models[38], where available, provide an optimal platform for ligand discovery and target validation. Herein, we provide comparable evidence supporting the BRD4–NUT fusion as a therapeutic target in an incurable, genetically-defined human squamous carcinoma, using a novel BRD4-directed small-molecule inhibitor.

Beyond NUT-midline carcinoma, BET-family bromodomains contribute to other neoplastic and non-neoplastic diseases. BRD4 targets the P-TEFb complex to mitotic chromosomes, resulting in the expression of growth-promoting genes such as *c-Myc*[12,14] and the well-established cancer target Aurora B[39]. BET family members have been recognized as essential genes for the replication of viruses[40,41] and in mediating inflammatory responses[42]. Thus, the availability of (+)-JQ1 will prompt informative research broadly in developmental and disease biology. JQ1 possesses many desirable qualities of a chemical probe, such as high target potency in homogeneous and cellular assays, a well-characterized profile of selectivity, synthetic accessibility and herein proven utility in experimental biology[18,19]. We have also found JQ1 to exhibit few off-target effects on cellular receptors and excellent pharmacokinetic properties including 49% oral bioavailability (Supplementary Figs 16 and 17 and Supplementary Table 5), establishing the plausibility of developing drug-like derivatives for therapeutic application.

The discovery and optimization of small-molecule inhibitors of epigenetic targets is a major focus of current biomedical research[43]. We sought to meet the challenge of developing potent, selective inhibitors of epigenetic readers. Here we present a first, thoroughly characterized

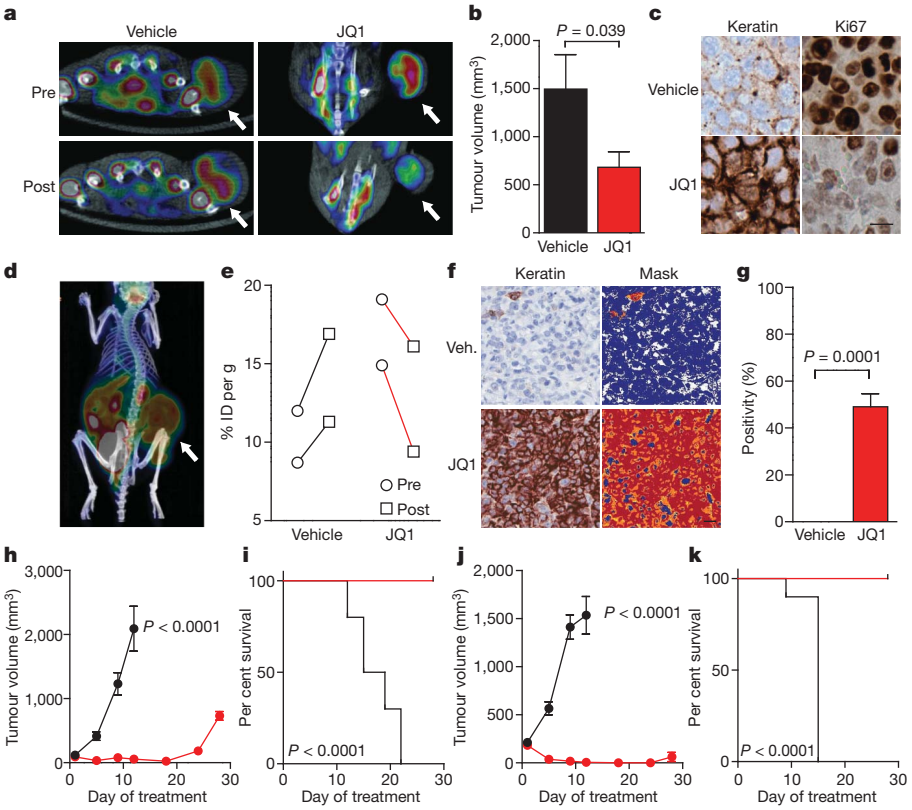

Figure 5 | JQ1 promotes differentiation, tumour regression and prolonged survival in murine models of NMC. **a**, PET imaging of murine NMC 797 xenografts. FDG uptake in xenograft tumours is reduced by 50 mg kg^{-1} JQ1 treatment compared to vehicle control. Arrows indicate the anatomical location of tumour xenograft. **b**, Tumour volume is reduced in mice with established disease (NMC 797 xenografts) treated daily with 50 mg kg^{-1} JQ1 compared to vehicle control. A significant response to therapy is observed by a two-tailed *t*-test at 14 days ($P = 0.039$). Data represent the mean ± s.d. ($n = 7$). **c**, Histopathological analysis of NMC 797 tumours excised from animals treated with JQ1 reveals induction of keratin expression (mouse anti-cytokeratin clone AE1/AE3, ×40) and impaired proliferation (Ki67, ×40), as compared to vehicle-treated animals (scale bar is 20 μm). **d**, Viability of patient-derived NMC 11060 xenografts was confirmed by PET imaging. Arrow indicates the anatomical location of tumour xenograft. **e**, Therapeutic response of primary 11060 NMC xenografts to (+)-JQ1 (50 mg kg^{-1} daily for 4 days) was demonstrated by PET imaging. Integrated signal encompassed within the tumour volume is presented as the per cent injected dose per gram (% ID per g). **f**, Histopathological analysis of primary NMC 11060 tumours excised from animals treated with (+)-JQ1 reveals induction of keratin expression (mouse anti-cytokeratin clone AE1/AE3, ×20; scale bar is 20 μm), compared to vehicle-treated animals. Quantitative analysis of keratin induction was performed using image masking (**f**, right panel) and pixel positivity analysis (**g**). A significant response to therapy is observed by a two-tailed *t*-test ($P = 0.0001$). Data represent the mean ± s.d. of three independent wide microscopic fields. Comparative images of stained excised tumours and quantitative masks are provided in Supplementary Fig. 14. **h**–**k**, (+)-JQ1 (red circles and lines; 50 mg kg^{-1} daily for 18 days) produces a decrease in tumour volume (**h**, **j**) and promotes prolonged survival (**i**, **k**) in patient-derived 11060 (**h**, **i**) and Per403 (**j**, **k**) NMC xenograft models ($n = 10$ in all groups). A significant response to therapy is observed for tumour volume by a two-tailed *t*-test ($P < 0.0001$) and for overall survival by a log-rank test ($P < 0.0001$). Black circles and lines, vehicle.

inhibitor of the BET-family of bromodomains. The approach outlined herein further establishes the feasibility of abrogating protein–protein interactions with small molecules, and targeting additional epigenetic readers for ligand discovery.

METHODS SUMMARY

The inhibitor JQ1 was synthesized in both racemic and enantiomerically pure format using the synthetic route outlined in scheme 1 and scheme 2 (Supplementary Methods) and its structure was fully characterized. Human bromodomains were expressed in bacteria as His-tagged proteins and were purified by nickel-affinity and gel-filtration chromatography. Protein integrity was assessed by SDS–PAGE and electro-spray mass spectrometry on an Agilent 1100 Series LC/MSD TOF. All crystallizations were carried out at 4 °C using the sitting-drop vapour-diffusion method. X-ray diffraction data were collected at the Swiss Light source beamline X10SA, or using a Rigaku FR-E generator. Structures were determined by molecular replacement. Isothermal titration calorimetry experiments were performed at 15 °C on a VP-ITC titration microcalorimeter (MicroCal). Thermal melting experiments were carried out on an Mx3005p RT–PCR machine (Stratagene) using SYPRO Orange as a fluorescence probe. Dose-ranging small-molecule studies of proliferation were performed in white, 384-well plates (Corning) in DMEM media containing 10% FBS. Compounds were delivered with a JANUS pin-transfer robot and proliferation measurements were made on an Envision multilabel plate-reader (PerkinElmer). Murine xenografts were established by injecting NMC cells in 30% Matrigel (BD Biosciences) into the flank of 6-week-old female NCr nude mice (Charles River Laboratories). Tumour measurements were assessed by caliper measurements, and volume was calculated using the formula $\mathrm{Vol} = 0.5 \times L \times W^2$. All mice were humanely killed, and tumours were fixed in 10% formalin for histopathological examination. Quantitative immunohistochemistry was performed using the Aperio Digital Pathology Environment (Aperio Technologies) at the DF/HCC Core Laboratory at the Brigham and Women's Hospital.

Received 5 May; accepted 17 September 2010.
Published online 24 September 2010.

1. Ptashne, M. Binding reactions: epigenetic switches, signal transduction and cancer. *Curr. Biol.* **19,** R234–R241 (2009).
2. Schreiber, S. L. & Bernstein, B. E. Signaling network model of chromatin. *Cell* **111,** 771–778 (2002).
3. Marushige, K. Activation of chromatin by acetylation of histone side chains. *Proc. Natl Acad. Sci. USA* **73,** 3937–3941 (1976).
4. Dey, A., Nishiyama, A., Karpova, T., McNally, J. & Ozato, K. Brd4 marks select genes on mitotic chromatin and directs postmitotic transcription. *Mol. Biol. Cell* **20,** 4899–4909 (2009).

5. Owen, D. J. *et al.* The structural basis for the recognition of acetylated histone H4 by the bromodomain of histone acetyltransferase gcn5p. *EMBO J.* **19,** 6141–6149 (2000).
6. Zeng, L. & Zhou, M. M. Bromodomain: an acetyl-lysine binding domain. *FEBS Lett.* **513,** 124–128 (2002).
7. Yang, X. J. Multisite protein modification and intramolecular signaling. *Oncogene* **24,** 1653–1662 (2005).
8. Yang, Z. *et al.* Recruitment of P-TEFb for stimulation of transcriptional elongation by the bromodomain protein Brd4. *Mol. Cell* **19,** 535–545 (2005).
9. Peng, J., Zhu, Y., Milton, J. T. & Price, D. H. Identification of multiple cyclin subunits of human P-TEFb. *Genes Dev.* **12,** 755–762 (1998).
10. Marshall, N. F. & Price, D. H. Purification of P-TEFb, a transcription factor required for the transition into productive elongation. *J. Biol. Chem.* **270,** 12335–12338 (1995).
11. Marshall, N. F., Peng, J., Xie, Z. & Price, D. H. Control of RNA polymerase II elongation potential by a novel carboxyl-terminal domain kinase. *J. Biol. Chem.* **271,** 27176–27183 (1996).
12. Phelps, M. A. *et al.* Clinical response and pharmacokinetics from a phase 1 study of an active dosing schedule of flavopiridol in relapsed chronic lymphocytic leukemia. *Blood* **113,** 2637–2645 (2009).
13. Rahl, P. B. *et al.* c-Myc regulates transcriptional pause release. *Cell* **141,** 432–445 (2010).
14. Yang, Z., He, N. & Zhou, Q. Brd4 recruits P-TEFb to chromosomes at late mitosis to promote G1 gene expression and cell cycle progression. *Mol. Cell. Biol.* **28,** 967–976 (2008).
15. French, C. A. *et al.* BRD4 bromodomain gene rearrangement in aggressive carcinoma with translocation t(15;19). *Am. J. Pathol.* **159,** 1987–1992 (2001).
16. French, C. A. *et al.* BRD4-NUT fusion oncogene: a novel mechanism in aggressive carcinoma. *Cancer Res.* **63,** 304–307 (2003).
17. French, C. A. *et al.* BRD-NUT oncoproteins: a family of closely related nuclear proteins that block epithelial differentiation and maintain the growth of carcinoma cells. *Oncogene* **27,** 2237–2242 (2008).
18. Frye, S. V. The art of the chemical probe. *Nature Chem. Biol.* **6,** 159–161 (2010).
19. Oprea, T. I. *et al.* A crowdsourcing evaluation of the NIH chemical probes. *Nature Chem. Biol.* **5,** 441–447 (2009).
20. Miyoshi, S., Ooike, S., Iwata, K., Hikawa, H. & Sugaraha, K. Antitumor agent. International Patent No. PCT/JP2008/073864 (WO/2009/084693) (2009).
21. Adachi, K. *et al.* Thienotriazolodiazepine compound and a medicinal use thereof. International Patent No. PCT/JP2006/310709 (WO/2006/129623) (2006).
22. Sueoka, H., Komatsu, H., Kobayashi, H. & Ehara, S. *Thienotriazolodiazepine Compounds and Medicinal Uses Thereof* 1–50 (Yoshitomi Pharmaceutical Industries, Ltd, 1998).
23. VonVoigtlander, P. F. & Straw, R. N. Alprazolam: Review of pharmacological, pharmacokinetic and clinical data. *Drug Dev. Res.* **6,** 1–12 (1985).
24. Niesen, F. H., Berglund, H. & Vedadi, M. The use of differential scanning fluorimetry to detect ligand interactions that promote protein stability. *Nature Protocols* **2,** 2212–2221 (2007).
25. Fedorov, O. *et al.* A systematic interaction map of validated kinase inhibitors with Ser/Thr kinases. *Proc. Natl Acad. Sci. USA* **104,** 20523–20528 (2007).
26. Bullock, A. N. *et al.* Structural basis of inhibitor specificity of the human protooncogene proviral insertion site in moloney murine leukemia virus (PIM-1) kinase. *J. Med. Chem.* **48,** 7604–7614 (2005).
27. Quinn, A. M. *et al.* A homogeneous method for investigation of methylation-dependent protein-protein interactions in epigenetics. *Nucleic Acids Res.* **38,** e11 (2010).
28. Vollmuth, F., Blankenfeldt, W. & Geyer, M. Structures of the dual bromodomains of the P-TEFb-activating protein Brd4 at atomic resolution. *J. Biol. Chem.* **284,** 36547–36556 (2009).
29. Dey, A. *et al.* A bromodomain protein, MCAP, associates with mitotic chromosomes and affects G_2-to-M transition. *Mol. Cell. Biol.* **20,** 6537–6549 (2000).
30. Huang, M. E. *et al.* Use of all-trans retinoic acid in the treatment of acute promyelocytic leukemia. *Blood* **72,** 567–572 (1988).
31. Druker, B. J. *et al.* Efficacy and safety of a specific inhibitor of the BCR-ABL tyrosine kinase in chronic myeloid leukemia. *N. Engl. J. Med.* **344,** 1031–1037 (2001).
32. Haack, H. *et al.* Diagnosis of NUT midline carcinoma using a NUT-specific monoclonal antibody. *Am. J. Surg. Pathol.* **33,** 984–991 (2009).
33. Toretsky, J. A. *et al.* Translocation (11;15;19): a highly specific chromosome rearrangement associated with poorly differentiated thymic carcinoma in young patients. *Am. J. Clin. Oncol.* **26,** 300–306 (2003).
34. Buchdunger, E. *et al.* Selective inhibition of the platelet-derived growth factor signal transduction pathway by a protein-tyrosine kinase inhibitor of the 2-phenylaminopyrimidine class. *Proc. Natl Acad. Sci. USA* **92,** 2558–2562 (1995).
35. Buchdunger, E. *et al.* Inhibition of the Abl protein-tyrosine kinase *in vitro* and *in vivo* by a 2-phenylaminopyrimidine derivative. *Cancer Res.* **56,** 100–104 (1996).
36. Schindler, T. *et al.* Structural mechanism for STI-571 inhibition of abelson tyrosine kinase. *Science* **289,** 1938–1942 (2000).
37. Druker, B. J. *et al.* Effects of a selective inhibitor of the Abl tyrosine kinase on the growth of Bcr-Abl positive cells. *Nature Med.* **2,** 561–566 (1996).
38. le Coutre, P. *et al. In vivo* eradication of human BCR/ABL-positive leukemia cells with an ABL kinase inhibitor. *J. Natl Cancer Inst.* **91,** 163–168 (1999).
39. You, J. *et al.* Regulation of aurora B expression by the bromodomain protein Brd4. *Mol. Cell. Biol.* **29,** 5094–5103 (2009).
40. You, J. *et al.* Kaposi's sarcoma-associated herpesvirus latency-associated nuclear antigen interacts with bromodomain protein Brd4 on host mitotic chromosomes. *J. Virol.* **80,** 8909–8919 (2006).
41. Abbate, E. A., Voitenleitner, C. & Botchan, M. R. Structure of the papillomavirus DNA-tethering complex E2:Brd4 and a peptide that ablates HPV chromosomal association. *Mol. Cell* **24,** 877–889 (2006).
42. Huang, B., Yang, X. D., Zhou, M. M., Ozato, K. & Chen, L. F. Brd4 coactivates transcriptional activation of NF-κB via specific binding to acetylated RelA. *Mol. Cell. Biol.* **29,** 1375–1387 (2009).
43. Cole, P. A. Chemical probes for histone-modifying enzymes. *Nature Chem. Biol.* **4,** 590–597 (2008).

Supplementary Information is linked to the online version of the paper at www.nature.com/nature.

Acknowledgements We are grateful to U. Oppermann, S. Müller, S. Sallan, C. Lathan, P. Rahl, R. Young, K. Lee and K. Shaw for discussions and sharing unpublished information; K. Agu, S. Johnston and L. Li for analytical chemistry support; J. Daley for flow cytometry support; T. Bowman, T. Caron, C. Marvin and S. Rodig for immunohistochemistry; and A. Bass for sharing cell lines. The Structural Genomics Consortium is a registered charity (number 1097737) that receives funds from the Canadian Institutes for Health Research, the Canadian Foundation for Innovation, Genome Canada through the Ontario Genomics Institute, GlaxoSmithKline, Karolinska Institutet, the Knut and Alice Wallenberg Foundation, the Ontario Innovation Trust, the Ontario Ministry for Research and Innovation, Merck & Co., Inc., the Novartis Research Foundation, the Swedish Agency for Innovation Systems, the Swedish Foundation for Strategic Research and the Wellcome Trust. This research was supported by a Graduate Fellowship from the Chemistry-Biochemistry-Biology Interface Program at the University of Notre Dame, NIGMS T32-075762 (to Y.S.), the DF/HCC (to C.A.F. and J.E.B.), the National Institutes of Health, the Burroughs Wellcome Fund, and the Leukemia & Lymphoma Society (to J.E.B.).

Author Contributions P.F., J.Q., S.K. and J.E.B. designed the study, analysed data and wrote the manuscript. P.F. and S.P. performed and analysed biophysical studies. J.Q. and J.E.B. designed JQ1 and established the synthetic routes. Y.S. and O.W. completed docking and molecular dynamics studies. O.F. performed and analysed DSF. S.M. and N.L.T. contributed biochemical assays. M.R.M., M.P. and T.D.H. performed and analysed alpha-screen assays. W.B.S., M.J.C. and J.E.B. performed *in vitro* NMC studies and immunohistochemistry. E.M.M. performed flow cytometry studies. E.M.M. and N.W. performed proliferation studies. T.T.H., M.J.C., C.A.F. and J.E.B. completed FRAP studies. M.R.M. and B.S. performed expression analysis. Y.W., A.L.C. and A.L.K. completed *in vivo* efficacy studies. T.K. and I.F. expressed and purified proteins. S.K. and J.E.B. supervised the research.

Author Information Atomic coordinates and structure factors for the reported crystal structures have been deposited with the Protein Data Bank under accession codes 2OSS (BRD4(1)), 3MXF (BRD4(1)–(+)-JQ1) and 3ONI (BRD2(2)–(+)-JQ1). Reprints and permissions information is available at www.nature.com/reprints. The authors declare no competing financial interests. Readers are welcome to comment on the online version of this article at www.nature.com/nature. Correspondence and requests for materials should be addressed to S.K. (stefan.knapp@sgc.ox.ac.uk) or J.E.B. (james_bradner@dfci.harvard.edu).